PHYSICAL REVIEW A **96**, 032704 (2017)

Dissociative ionization of the H_2O molecule induced by medium-energy singly charged projectiles

S. T. S. Kovács,* P. Herczku, Z. Juhász, L. Sarkadi, L. Gulyás, and B. Sulik
Institute for Nuclear Research, Hungarian Academy of Sciences (MTA Atomki), P.O. Box 51, H-4001 Debrecen, Hungary
(Received 9 June 2017; revised manuscript received 1 August 2017; published 7 September 2017)

We report on the fragmentation of the water molecule by 1 MeV H^+ and He^+ and 650 keV N^+ ion impact. The fragment-ion energy spectra were measured by an electrostatic spectrometer at different observation angles. The obtained double-differential fragmentation cross sections for N^+ are found to be more than an order of magnitude higher than that for H^+. The relative ratios of the fragmentation channels are also different for the three projectiles. Additional fragmentation channels were observed in the spectra for He^+ and for N^+ impact, which are missing in the case of H^+. From the analysis of the kinetic energy of the fragments, the maximum observed degree of ionization was found to be $q_{max} = 3$, 4, and 5 for H^+, He^+, and N^+ impact, respectively. Absolute multiple-ionization cross sections have been determined. They are compared with the predictions of the classical trajectory Monte Carlo and continuum-distorted-wave eikonal-initial-state theories. At lower degrees of ionization, theories provide reasonable agreement with experiment. The systematic overestimation of the cross section by the theories towards higher degrees of ionization indicates the failure of the independent particle model.

DOI: 10.1103/PhysRevA.96.032704

I. INTRODUCTION

The dissociation of small few-atom molecules has been extensively studied by the impact of various types of projectiles, such as photons [1–3], electrons [4,5], protons [6–8], and multiply charged ions [9–13]. Molecular fragmentation by ion impact is a rather complex process, which is highly interesting in different areas from astrophysics to cancer therapy. In these fields the most interesting impact energy region is the surrounding of the so-called Bragg peak, where the energy transfer to the medium maximizes [14–16]. The equilibrium charge state of the projectile ions in the distal region (low-energy side) of the Bragg peak is usually close to unity in a wide kinetic energy range; e.g., heavier ions are strongly screened there [17]. In spite of their relevance, systematic studies in the Bragg-peak region with dressed-ion projectiles are rather scarce. In one of those works Montenegro *et al.* [14] found that the fragmentation yield does not follow the steep decrease of the linear energy transfer (LET) at the low-energy side of the Bragg peak. The dissociation yield has been found practically constant down to very low projectile energies.

The fragmentation pattern of a target molecule is determined by the velocity, charge state, and structure of the projectile [10] and the open fragmentation channels taking place in the reaction [9]. By the collision, the target molecule may fall to several possible excited and ionized states. Some of those states of the transient (i.e., precursor) molecular ion will initiate dissociation into the open fragmentation channels. Multiple-vacancy states are particularly dissociative. Multiple electron removal from the target molecule can happen, e.g., by direct multiple ionization, by transfer ionization, or by single ionization followed by secondary processes. Scully *et al.* [18] showed that the role of secondary Auger processes is non-negligible in producing multiply charged molecular ions even in the case of electron impact. The emitted fragments can be neutral or charged particles in excited or ground states [7]. There are also two- or three-step fragmentation processes [7,10,19], i.e., sequential dissociations such as $H_2O^{2+} \rightarrow OH^+ + H^+ \rightarrow O^+ + H^+ + H^0$. Note that a fragmentation channel is usually characterized by the charge states of the precursor ion and the fragments, without specifying their electronic, vibrational, or rotational states. Accordingly, the same channel notation may be used for a set of subchannels with different kinetic energy release (KER) values.

The kinetic energy release is typically low for ion-neutral breakups. For few-atom molecules, it is often only a few tenths of an eV, and the upper limit is around 5 eV. For breakups involving at least two positive ions the region of KER extends up to much higher energies: it is between about 3 and 100 eV [19]. The higher KER for the latter case is due to the Coulomb repulsion between the charged fragments, which increases with the charge state of the transient molecular ion (Coulomb explosion) [11,20]. For the accurate determination of the KER distribution one has to take into account the electronic excitation of the transient molecular ion and the emergent fragments [20,21], as well as the rotational and vibrational degrees of freedom of the precursor molecular ion [11,12]. The several possible excited states of the precursor molecular ion and the emergent fragments result in a spread of the kinetic energies of the fragments originating from the same dissociation channel. Furthermore, the kinetic energy distribution for a certain fragmentation channel may differ in the case of one-, two-, or three-step processes [7,19]. As a result, the fragment energy spectra are rather complex.

In most of the experiments, the dissociation pattern of water was studied thoroughly only for the low-charge-state transient molecular ion (H_2O^{q+}, where $q \leqslant 3$) [4,5,9,10,14,15,22,23]. In a recent work Pedersen *et al.* [2] studied the dissociation of the H_2O^{2+} molecular ion in detail, induced by XUV photons from H_2O^+ ions. They devoted special attention to the excited states of the initial molecular ion and the emitted fragments, and their effect on the KER distribution. Higher ionization states of the water molecule were observed in collisions with slow, highly charged ions (HCIs) [12,13,24–26], where

*kovacs.sandor@atomki.mta.hu

the dominant ionization process is multiple electron capture. Here the degree of target ionization strongly depends on the initial charge of the projectile: The maximal degree of target ionization was found to be $q = 4$, 5, and 8 by different groups utilizing Ne^{7+} [13], Ar^{9+} [12], and Xe^{44+} [26], respectively. Recently Wolff and co-workers [27] observed higher degrees of ionization of the water molecule ($q = 4$,5) by the impact of MeV-energy ions.

For heavier ions only relatively few works [14,27] cover both the charge state and energy ranges, which are typical for the close surrounding and the distal region of the Bragg peak. In the present work we concentrate on this relevant but less investigated area. We study the emission of fragments from the multiple ionization of water, while bombarding it with medium-energy, single charged atomic-ion projectiles. These projectiles mostly interact with the target molecule by weak, screened Coulomb potential. Direct single ionization is the dominant process here, even for the slowest ($v = 1.4$ a.u.) N^+ projectile. Classical and quantum-mechanical calculations confirm that in such collision systems, the electron emission spectrum is dominated by electrons from single ionization [28]. We note that only a smaller fraction of the H_2O^+ molecular ions is expected to dissociate. For charged-particle impact the dissociating fraction was found to be around 30% both theoretically and experimentally [18,26].

In close collisions, the perturbation strength for "dressed" projectiles may approach that for bare projectiles. This is due to the rapidly decreasing screening effect of the projectile electrons towards smaller impact parameters. In such close collisions the effective charge exceeds the ionic charge for a short time period [29], and the target feels strong perturbation. Such collision events can produce remarkable double- and multiple-ionization yields even for neutral-atom impact [30]. Though their contributions may remain low compared with single ionization, they are responsible for the production of the majority of the fragments in the 3–100-eV fragment energy range. Fragment energies from the breakup of H_2O^+ are below 3 eV [10]. The connection between the primary ionization and the subsequent molecular fragmentation has been the subject of numerous studies for lower degrees of ionization [7,10,26]. As the degree of ionization becomes higher with increasing perturbation, several new fragmentation channels open. Thus, fragmentation measurements offer a sensitive method for studying multiple ionization of molecules.

In this work we measured double-differential fragment-ion emission spectra for the gas-phase H_2O molecule by the impact of H^+, He^+, and N^+ ions. From the spectra we determined absolute cross sections for the individual fragmentation channels. The latter procedure is based on extensive earlier studies performed by several research groups [2,10–13,15,22–26], in which the overwhelming majority of the fragmentation channels have been identified and their KER data have been determined, dominantly for H^+, He^{q+}, and HCI projectiles. From the cross sections determined for the individual fragmentation channels we deduced the multiple-ionization cross sections for the target molecule. The experimental results are analyzed by comparing them with the predictions of the continuum-distorted-wave eikonal-initial-state (CDW-EIS) and the classical trajectory Monte Carlo (CTMC) theories.

II. EXPERIMENT

The fragmentation of the H_2O molecule was investigated in a standard crossed beam experiment in Atomki, Debrecen [28]. Beams of H^+, He^+, and N^+ were provided by a 5-MV Van de Graaff (VdG) accelerator with energies 1 MeV/nucleon, 250 keV/nucleon, and 46 keV/nucleon, respectively.

The ion beams were guided through a 15° deflector chamber in order to keep the charge state of the ions well defined. After the deflector chamber two pairs of electrostatic steerers were mounted in the beam line as fine-tuning elements. Collimation of the ion beam was performed by a four-jawed slit placed 120 cm from the entrance of the experimental chamber, and a somewhat larger aperture between the four-jawed slit and the chamber. During beam tuning a precisely aligned additional aperture was temporarily placed just after the entrance of the experimental chamber. This aperture was removed during the measurements. The beam current was measured by a two-stage differential Faraday cup. A double-layer magnetic shielding reduced the magnetic field to a few milligauss in the scattering chamber.

A jet of H_2O vapor was led into the experimental chamber through a 1-mm-diam nozzle. A pressure regulator with an automatically operated needle valve ensured constant buffer pressure and continuous gas flow regulation. The container of the prepurified, carbon-free liquid water was attached to the entrance of this pressure-regulating system. Dissolved gases were carefully pumped out. The target gas density in the collision volume was 2×10^{13} cm^{-3}. The continuous background pressure was around 9×10^{-7} and 1×10^{-5} mbar without and with target gas inlet, respectively.

The cylindrical scattering chamber of 1000 mm diameter was equipped with rotatable rings. Charged fragments ejected from the collisions were energy analyzed by a single-stage energy-dispersive electrostatic spectrometer fixed on one of the rings. The experimental geometry allowed us to measure the angular distribution of the fragments from 20° to 160° relative to the incident ion beam. In order to avoid recombinations caused by the background gases, we used a small, compact spectrometer, close to the collision region. The pass length from the collision center to the channeltron detector was less than 10 cm. The base energy resolution of the spectrometer was 3%.

Fragment ion energy spectra at different observation angles were taken from 0.4 to 200 eV. Absolute double-differential fragmentation cross sections were obtained by a standard normalization procedure. The effective target length and target gas density have been evaluated by the procedure given in Refs. [28,31]. The transmission of the spectrometer was determined from its geometrical parameters. The charged fragments were accelerated before they entered the channeltron detector by applying 1 kV potential between the exit slit of the analyzer and the entrance of the channeltron. The efficiency of the channeltron detector ($\eta = 0.85 \pm 0.08$) for these ions was taken from the literature [32].

The statistical error was estimated less than 20% for H^+ impact, and far below 10% for He^+ and N^+ projectiles in the main, structured region of the spectra (typically in the energy ranges 3–15, 3–30, and 3–50 eV for proton, helium, and nitrogen ion impact, respectively). The systematic error

was estimated around 25% in these energy regions, mostly due to the uncertainty of the detection efficiency. Thus the overall accuracy of the cross-section data in the structured region is $\leqslant 30\%$. Below 3 eV we estimate the systematic error somewhat higher (about 40%) due to the charging of the oxidized surfaces of the spectrometer. Therefore, the overall accuracy goes up to 40–50 % here. At higher energies, near the end of the spectra, the overall uncertainty also increases due to the increasing statistical error.

III. THEORETICAL CONSIDERATIONS

In a previous work [28] we studied the present collision systems by measuring and analyzing the energy spectra of the emitted electrons. There the electron emission cross sections were compared with the results of CDW-EIS and CTMC calculations, extended to treat molecular orbitals and screened potentials for describing the electron emission from molecules impacted by dressed projectiles. The details of the theories can be found in Refs. [28,33–35].

Briefly, the CDW-EIS model is a first-order method which proved to be very successful for describing atomic collisions at medium and high impact energies [36,37] and its extension to molecular collisions are provided in Refs. [26,34,38,39]. When the projectile has no electron(s), the effect of the projectile on the unperturbed atomic or molecular orbitals is taken into account by using eikonal and Coulomb distorted-wave functions, respectively, for the initial and final channels. The process where the projectiles bring electron(s) into the collision has been considered by Monti *et al.* [40] for describing atomic collisions with dressed projectiles. The interaction between the projectile and the active electron has been written as a short-range potential term plus a long-range term due to the asymptotic screened projectile charge q. The projectile's distortion, as for the pure Coulomb case, is still considered by a bare ion with charge q and the short-range interaction was taken into account by a first-order matrix element in the transition amplitude. The same idea has been applied in our description of molecular collisions with non-Coulomb projectiles. Therefore, the validity of the model, regarding the dynamics, can be judged on its capacities for describing atomic collisions.

The present CTMC model is an extended version of the standard three-body procedure used for ion-atom collisions. As a most important modification of the atomic theory, we apply a multicenter molecular potential to describe the interaction of the projectile and the electron with the molecular target core. In many aspects our model is similar to that of Illescas *et al.* [41]. However, unlike the latter authors, we describe the full three-body dynamics; i.e., we do not use the straight-line approximation for the projectile's path. The multicenter molecular potential is constructed as a sum of screened atomic potentials centered at the nuclei of the molecule. For the atomic and ionic potentials we apply the Green-Sellin-Zachor (GSZ) potential [42] with suitably chosen screening parameters [43]. The modification of the atomic potentials in the molecular environment is taken into account by changing one of the parameters of the GSZ potential, namely, the number of the electrons. The GSZ potential is used also for the collisions with dressed projectiles interacting via partially screened Coulomb potential. For the generation of the initial values of the position and momentum coordinates of the electron we follow the method suggested by Reinhold and Falcón [44] for isotropic non-Coulombic systems. Our method is a generalization of that proposed by the latter authors for the case of nonisotropic potentials. We note that due to the multicenter molecular potential, our model takes into account the multiple scattering effects of both the projectile and the electrons at the molecular centers. As a result, we consider it a more realistic description of the ion-molecule collisions than those which simply determine the collision properties (ionization and capture probabilities, and cross sections) as independent sums of the individual atomic contributions.

In the present work we use the same models to describe multiple ionization of the H_2O molecule, leading to molecule fragmentation. For the treatment of the multiple-vacancy production in the framework of the independent particle model (IPM), the impact-parameter formulation is used. For a specific molecular orbital (MO) the calculations yield impact-parameter-dependent single-electron probabilities for ionization, $p_i(b)$, and electron capture, $p_c(b)$. We note that for molecules the impact parameter is a vector in the plane, which is perpendicular to the projectile trajectory. Moreover, the probabilities are both impact-parameter and orientation dependent.

The multiple-vacancy production, when n electrons are ejected and m are captured to the projectile from the initial number of electrons, N, on a specific MO, is given by the following multinomial expression:

$$P_{i^n c^m} = \binom{N}{n}\binom{N-n}{m} p_i^n \, p_c^m \, (1 - p_i - p_c)^{N-(n+m)}. \quad (1)$$

For a molecule having Q MOs, the probability of multiple-vacancy creation is a product of the contributions of the individual MOs. The probability of creating the $(n_1,n_2,\ldots,n_Q;m_1,m_2,\ldots,m_Q)$ vacancy configuration is given by

$$P_{i^{n_1,n_2,\ldots n_Q} c^{m_1,m_2,\ldots m_Q}} = \prod_{k=1}^{Q} \binom{N_k}{n_k}\binom{N_k-n_k}{m_k} p_{ik}^{n_k} \, p_{ck}^{m_k} \, (1-p_{ik}-p_{ck})^{N_k-(n_k+m_k)}, \quad (2)$$

where $k = 1,\ldots,Q$; N_k is the number of the electrons on the kth MO; p_{ik} and p_{ck} are the ionization and capture probabilities from the kth MO, respectively; and n_k and m_k are the numbers of ejected and captured electrons, respectively, from orbital k.

IV. RESULTS AND DISCUSSIONS

Typical fragment ion energy spectra measured in the present work are displayed in Fig. 1. The fragment ion emission is found to be isotropic. Therefore, in Fig. 1 we show spectra taken at just one particular observation angle ($\theta = 45^\circ$). They exhibit significant differences for the three projectiles. The cross section significantly increases with increasing atomic number of the projectile. This can be attributed to the increasing perturbation strength from H^+ to N^+, characterized by the Bohr-Sommerfeld parameter, $\delta = q/v$, i.e., the ratio

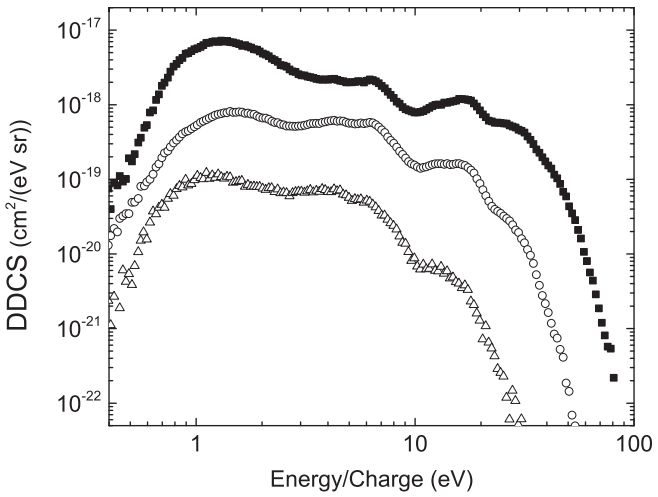

FIG. 1. Absolute double-differential fragmentation cross-section spectra for the H_2O molecule measured at 45° observation angle. Open triangles stand for H^+ impact, open circles for He^+, and solid squares for the N^+ projectile. The yields above 15 eV are due to multiple-ionization ($q > 2$) processes. Their relative contribution is small for H^+ and strongly increases with increasing perturbation (see text).

of the projectile charge to its velocity (in atomic units). Its values are 0.16, 0.63, and 0.74 for H^+, He^+, and N^+ impact, respectively [28]. Concerning multiple ionization, the effective perturbation becomes even stronger with increasing nuclear charge due to the weaker screening of the projectile nucleus at small impact parameters. Indeed, the cross section is about one order of magnitude higher for He^+, and two orders of magnitude higher for N^+ than that for H^+ impact. The structure of the spectra also changes significantly with increasing perturbation strength. The relative yields for the $q > 2$ multiple-ionization events (above 15 eV) are 3.6%, 18%, and 37% for the H^+, He^+, and N^+ projectiles, respectively.

For the identification of the measured fragmentation channels and fragment energies we relied on the KERs and individual fragment energies given in Refs. [2,10–13,45]. These values are summarized in Table I. In these studies the fragmentation pattern of the H_2O molecule was investigated by the impact of different projectiles. Pedersen *et al.* [2] studied the fragmentation of the H_2O^{2+} molecular ions by XUV photons in coincident measurements. Special attention was put on the different excited states of the precursor molecular ions and fragments and their effect on the measured spectra. Alvarado *et al.* [10] studied the fragmentation of water molecules induced by singly charged ion bombardment. Using the time-of-flight (TOF) technique, they measured the energy distribution of the fragments originating from the single, double, and triple ionization of the molecule. Fragments from the higher ionization states of the H_2O molecule were observed in collisions of water with slow HCIs by different groups [11–13]. In a recent work Wolff *et al.* [27] studied the fragmentation pattern of water by different ion projectiles (H^+, $Li^{0,\ldots,3+}$, C^+, and C^{2+}). Their fragmentation channel identification was based on a combination of Coulomb explosion and CTMC calculations (CE-CTMC) in reasonable agreement with their experimental results.

We detected only one of the fragments from each dissociation event. However, the fragmentation channels could be well identified in the measured spectra using the information found in the above-mentioned works. From the tabulated KER

TABLE I. Summary of the literature data used in the present analysis. The last column refers to the identification number of the peak, which stands for the fragmentation channel in Fig. 3 and Table II. The same number with different lower-case letters represent the components of one "collector" peak during the fit. For those fragmentation channels where only the KER values were directly available, we calculated the approximate H^+ energies denoted by *. The KER values 7.8 and 11.7 are pure theoretical data which are supported by the experimental results in Ref. [2] but have not been identified by other groups. The abbreviation "PIPICO" stands for the method of photoion-photoion coincidence spectroscopy.

Projectile	Method	Fragmentation channel	KER (eV)	FWHM (eV)	H^+ energy (eV)	H^+ FWHM (eV)	Ref.	Peak no.
6–23 keV H^+, He^+, He^{2+}	TOF	$H_2O^+ \rightarrow OH^0 + H^+$			2 ± 0.5		[10]	4
6–23 keV H^+, XUV	TOF, coincidence	$H_2O^{2+} \rightarrow OH^+ + H^+$	3.7 ± 0.5		3.5 ± 0.5		[2,10]	5a
6–23 keV He^+, XUV	TOF, coincidence	$H_2O^{2+} \rightarrow OH^+ + H^+$	4.0 ± 0.5		3.8 ± 0.5	~6 [10]	[2,10]	5b
He II	PIPICO	$H_2O^{2+} \rightarrow OH^+ + H^+$	4.5 ± 0.5		4.2*		[45]	5c
XUV, He II	Ion spectroscopy	$H_2O^{2+} \rightarrow O^+ + H^+ + H^0$	4.8 ± 1.0		~5		[13,45]	6a
XUV	Coincidence	$H_2O^{2+} \rightarrow OH^+ + H^+$	6 ± 2		5.6*		[2]	6b
1–5 keV He^{2+}	TOF, coincidence	$H_2O^{2+} \rightarrow OH^+ + H^+$	6.8 ± 1		6.5 ± 1	~6	[10]	7
XUV	Coincidence	$H_2O^{2+} \rightarrow OH^+ + H^+$	7.8		7.4*		[2]	8
XUV	Coincidence	$H_2O^{2+} \rightarrow OH^+ + H^+$	11.7		11.05*		[2]	9
6–23 keV H^+, He^+	TOF	$H_2O^{2+} \rightarrow O^+ + H^+ + H^0$	15.3 ± 1		14.5 ± 1	~15	[10]	10
6–23 keV He^{2+}	TOF	$H_2O^{3+} \rightarrow O^+ + H^+ + H^+$	36 ± 0.5		17.8 ± 0.5	~15	[10]	11a
20 keV HCI	TOF, ion spectroscopy	$H_2O^{3+} \rightarrow O^+ + H^+ + H^+$	~35		18 ± 1.0	~15	[11–13]	11b
6–23 keV He^{2+}	TOF	$H_2O^{3+} \rightarrow O^{2+} + H^+ + H^0$	~30		28 ± 0.5	~23	[10]	13a
20 keV HCI	Ion spectroscopy	$H_2O^{3+} \rightarrow O^{2+} + H^+ + H^0$			28 ± 1		[12,13]	13b
100–125 keV HCI	TOF	$H_2O^{4+} \rightarrow O^{2+} + H^+ + H^+$	~68	~20	32.6*		[11]	14
20 keV HCI	Ion spectroscopy	$H_2O^{4+} \rightarrow O^{3+} + H^+ + H^0$			~38		[13]	15
100–125 keV HCI	TOF	$H_2O^{5+} \rightarrow O^{3+} + H^+ + H^+$	~95	~28	45.4*		[11]	16

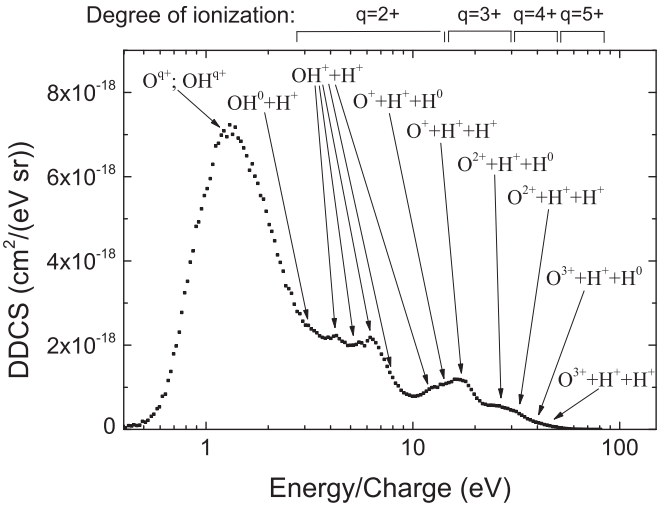

FIG. 2. Absolute double-differential fragmentation cross-section spectra of the H_2O molecule induced by 650-keV N^+ impact. The presented spectrum was measured at 45° observation angle. The identified fragmentation channels and the regions of the different ionization degrees are indicated.

values in Table I, one can estimate the kinetic energy of the individual fragments for ion-pair breakups by taking into account that the kinetic energies are inversely proportional to the masses of the fragments. Assuming that the neutrals carry a negligible fraction of KER [19], this estimation can be extended to ion-pair + neutral breakups, too. For the two ion triplets, where only the KER values are available (at 68 and 95 eV [11]), we relied on the analysis provided in the same work by Werner *et al.* [11] for the relative directions of the fragment momenta.

The identified fragmentation channels are shown in Fig. 2. The unresolved hump below 3 eV reflects mostly heavy fragments (O^{q+}, OH^{q+}) from ion-pair and ion-triplet breakups. A small amount of low-energy H^+ ions from ion-neutral breakups (single ionization of water) may also contribute to this region. In the case of ion-pair and ion-triplet breakups proton fragments produce a structured region above 3 eV. According to Fig. 2, the double-ionized water molecule dissociates mostly into two fragments. Protons from the $OH^+ + H^+$ channel produce an almost flat region from above 3 to 7 eV, and a more structured part between 7 and 12 eV. It contains several overlapping peaks, which belong to different excitation states of the transient H_2O^{2+} molecular ion and the emergent OH^+ fragments. Similar conclusions were drawn for the overlapping peaks in Refs. [2,10,11]. We note here that Refs. [2,12,13] predict a slight contribution of ion-pair + neutral channels to this energy region. The three-, four-, and fivefold-ionized molecules dominantly dissociate into ion triplets [10]. Protons from these highly ionized ($q > 2$) transient molecular ions appear above 15 eV.

A further analysis of the spectra in Fig. 1 revealed that the proton fragment peaks above 15 eV, appearing only for He^+ and N^+ projectiles, belong to the fragmentation channels which are due to the four- and fivefold ionization of the water molecule. In parallel with these proton peaks, the relative yield of the heavy fragments (<3 eV) also increases, which

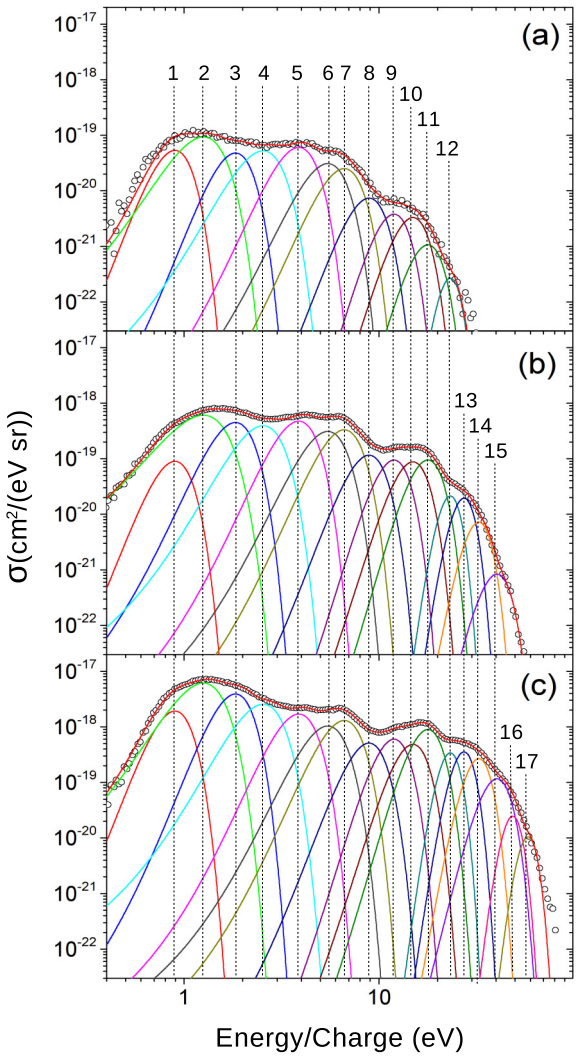

FIG. 3. Fragment ion spectra of H_2O induced by (a) H^+, (b) He^+, and (c) N^+ projectiles (symbols). The peaks represent Gaussian fit for the fragmentation channels listed in Tables I and II. Channel positions are indicated by vertical lines with numbers.

can be understood considering that light fragments have their corresponding heavy partners. From the maximum kinetic energy of the emitted protons, we concluded that the highest degree of ionization was $q_{\max} = 3$, 4, and 5 for H^+, He^+, and N^+ impact, respectively.

The fragmentation spectrum for N^+ impact observed in the present work is very similar to those reported in Refs. [13,25] measured by slow highly charged ions (see Fig. 3(b) in Ref. [13], and Figs. 2 and 3 in Ref. [25]). At first sight the perturbation exerted by the single charged nitrogen projectile seems to be surprisingly strong. The strong multiple-ionization capability of the dressed N^+ projectile can be attributed to the reduced screening of the projectile nucleus by its electrons in close collisions, i.e., at small N-O impact parameters, where multiple ionization is dominant. Accordingly, the effective charge for multiple ionization may exceed the ionic charge significantly.

For a quantitative analysis of the measured fragmentation patterns the spectra were decomposed to contributions from

TABLE II. The obtained cross sections (σ) of the individual fragmentation channels for the three projectiles. They are the results of the fit presented in Fig. 3. The energy center and FWHM values are the same for all projectiles. For peaks 1–3 these values correspond to the peaks containing different heavy fragments, while for peaks 4–17 the values correspond to H^+ fragments. The uncertainties include only the statistical errors and the estimated uncertainties of the fit.

Peak no.	Fragmentation channel	Center (eV)	FWHM (eV)	σ_{H^+} (cm^2)	σ_{He^+} (cm^2)	σ_{N^+} (cm^2)
1	Heavy (OH^{q+}; O^{q+})	0.89	0.35	$2.54 \pm 0.15 \times 10^{-19}$	$4.33 \pm 0.41 \times 10^{-19}$	$9.16 \pm 0.31 \times 10^{-18}$
2	Heavy (OH^{q+}; O^{q+})	1.25	0.65	$8.18 \pm 0.25 \times 10^{-19}$	$6.19 \pm 0.08 \times 10^{-18}$	$5.39 \pm 0.06 \times 10^{-17}$
3	Heavy (OH^{q+}; O^{q+})	1.83	0.74	$4.75 \pm 0.24 \times 10^{-19}$	$4.79 \pm 0.08 \times 10^{-18}$	$3.87 \pm 0.06 \times 10^{-17}$
4	$H_2O^+ \rightarrow OH^0 + H^+$	2.54	1.23	$8.66 \pm 0.27 \times 10^{-19}$	$6.49 \pm 0.08 \times 10^{-18}$	$4.21 \pm 0.05 \times 10^{-17}$
5	$H_2O^{2+} \rightarrow OH^+ + H^+$	3.87	1.68	$1.36 \pm 0.03 \times 10^{-18}$	$1.07 \pm 0.01 \times 10^{-17}$	$3.82 \pm 0.05 \times 10^{-17}$
6	$H_2O^{2+} \rightarrow OH^+ + H^+$	5.46	2.45	$1.02 \pm 0.05 \times 10^{-18}$	$1.02 \pm 0.02 \times 10^{-17}$	$3.40 \pm 0.09 \times 10^{-17}$
7	$H_2O^{2+} \rightarrow OH^+ + H^+$	6.63	2.83	$9.51 \pm 0.46 \times 10^{-19}$	$1.25 \pm 0.02 \times 10^{-17}$	$4.93 \pm 0.10 \times 10^{-17}$
8	$H_2O^{2+} \rightarrow OH^+ + H^+$	8.89	3.50	$3.46 \pm 0.23 \times 10^{-19}$	$5.43 \pm 0.10 \times 10^{-18}$	$2.40 \pm 0.07 \times 10^{-17}$
9	$H_2O^{2+} \rightarrow OH^+ + H^+$	11.94	4.22	$2.15 \pm 0.19 \times 10^{-19}$	$5.35 \pm 0.10 \times 10^{-18}$	$3.40 \pm 0.08 \times 10^{-17}$
10	$H_2O^{2+} \rightarrow O^+ + H^+ + H^0$	14.93	5.33	$2.37 \pm 0.20 \times 10^{-19}$	$6.27 \pm 0.14 \times 10^{-18}$	$3.47 \pm 0.11 \times 10^{-17}$
11	$H_2O^{3+} \rightarrow O^+ + H^+ + H^+$	17.83	6.11	$8.76 \pm 1.23 \times 10^{-20}$	$7.77 \pm 0.11 \times 10^{-18}$	$7.34 \pm 0.10 \times 10^{-17}$
12	$H_2O^{3+} \rightarrow$?	23.24	5.30	$1.91 \pm 0.34 \times 10^{-21}$	$1.51 \pm 0.05 \times 10^{-18}$	$2.42 \pm 0.06 \times 10^{-17}$
13	$H_2O^{3+} \rightarrow O^{2+} + H^+ + H^0$	27.30	6.59	$9.14 \pm 4.39 \times 10^{-22}$	$1.72 \pm 0.04 \times 10^{-18}$	$3.14 \pm 0.06 \times 10^{-17}$
14	$H_2O^{4+} \rightarrow O^{2+} + H^+ + H^+$	32.52	8.82		$8.53 \pm 0.28 \times 10^{-19}$	$3.17 \pm 0.06 \times 10^{-17}$
15	$H_2O^{4+} \rightarrow O^{3+} + H^+ + H^0$	40.36	12.75		$1.43 \pm 0.11 \times 10^{-19}$	$1.99 \pm 0.05 \times 10^{-17}$
16	$H_2O^{5+} \rightarrow O^{3+} + H^+ + H^+$	48.58	10.05			$3.32 \pm 0.22 \times 10^{-18}$
17	$H_2O^{5+} \rightarrow O^{4+} + H^+ + H^0$	58.22	11.67			$1.65 \pm 0.09 \times 10^{-18}$

particular fragmentation channels. The individual fits to the three spectra obtained by the different projectiles were coupled by an iterative process (see below) to achieve only one, common set of parameters for the channel energies and widths. The final fit curves together with the measured data are shown in Fig. 3. The fit is based on the data listed in Table I and on our channel identification (Fig. 2). The region of heavy fragments (<3 eV) is covered by three Gaussians. Their mean energies and FWHMs were varied to achieve the best fit with common values for all three projectiles. In the energy region of protons (>3 eV), each Gaussian represents an identified fragmentation channel. In addition to the data of Table I, one peak around 23.2 eV was necessary to insert for the best fit. Moreover, for the N^+ projectile an additional peak around 58 eV was necessary to add to the end of the spectrum. This peak is likely to be due to fragments from the highly excited, fivefold-ionized H_2O^{5+}* molecule. The energy center of the Gaussians was kept fixed during the fits of the first and last iterations. Data about the FWHM values are scarce in the literature. The few FWHM values for the individual channels presented in Table I have large uncertainties. Nevertheless, for charged-particle impact, these FWHM values are increasing with the channel energies. Therefore, to resolve the problem of the incomplete knowledge of the FWHM data, we started with the initial condition that the widths of the peaks are proportional to their energy centers. The initial value of the proportionality factor was set to 0.4. In the course of the iterative fitting procedure this factor was allowed to vary. As a result of the iteration it was finally found that the proportionality factor was around 0.4, 0.3, and 0.2 for channels of double, triple, and higher degrees of ionization, respectively.

In each step of the iterative fit procedure, we used a common set of initial values for the channel energies and widths for all the three spectra. During the three individual fits of the actual step the channel energies were allowed to vary within close limits (typically 1%, maximum 5% of the peak centers), while the limits were much larger for the FWHM values. From the results of the three fits of the actual iteration step, we extracted the initial channel energies and widths for the next step, again common for all three spectra. This procedure converged after eight iteration steps, for all the parameters. The results of the iterative fitting procedure are shown in Fig. 3 and in Table II. We found that the obtained channel energy values (given in Table II) were very close to the initial values of Table I.

We note that the fitted curves in the 4–12-eV energy region may contain slight contributions of fragmentation channels different from the identified components of the $OH^+ + H^+$ channel. According to the published experimental data, the $H_2O^{2+} \rightarrow O^+ + H^+ + H^0$ [12,13,45] channel also provides a small yield between 5 and 6 eV. Calculated data in Ref. [2] suggest that the $H_2O^{2+} \rightarrow O^0 + H^+ + H^+$ fragmentation channel may also contribute to the 4–12-eV region, but it has not been detected in any experimental work. As the articles report only small yields for these channels, the questioned energy region is attributed to the $OH^+ + H^+$ fragmentation channel in our work, characterized by slightly different KER values (see Table I).

The mean energies of the fragmentation channels of three-, four-, and fivefold ionization fall above 17 eV. They agree well with those calculated by the n-body CTMC (nCTMC) model of Wolff *et al.* [27]. Their channels denoted by "e" through "h" in Ref. [27] can be identified with our channels 13–16 in Table II, respectively. At lower energies the number of peaks in Ref. [27] is significantly smaller, though they can be identified with some of the peaks found in the present fittings. The reason is that many of the considered channels, taken from the literature, belong to excited states of the ionized precursor molecule, while no excitation is included in the model of Wolff *et al.* [27]. Nevertheless, their predicted energy positions are surprisingly good for the ground state of the precursor molecule ion.

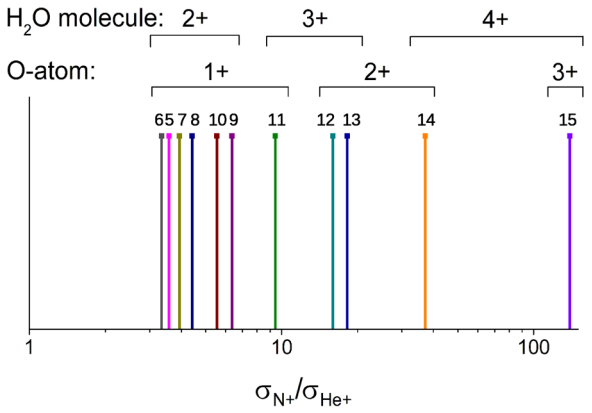

FIG. 4. The $\sigma_{N^+}/\sigma_{He^+}$ ratios for the individual fragmentation channels (the colors of the lines are the same as the colors of the Gaussians in Fig. 3). The ratios are presented starting from the $OH^+ + H^+$ channels. The sequence of the lines is almost the same as the sequence of the energy centers of the Gaussians. The ionization degrees of the H_2O molecule and the O fragments for the displayed channels are indicated.

The analysis of the obtained cross sections, presented in Table II, shows that the highest-energy fragmentation channels have almost two orders of magnitude lower yield than the double-ionization channels for all projectiles. The highest-energy proton fragments belong to the fragmentation channels of $O^{2+} + H^+ + H^0$, $O^{3+} + H^+ + H^0$, and $O^{4+} + H^+ + H^0$ for H^+, He^+, and N^+ impact, respectively.

Further analysis was made via the $\sigma_{N^+}/\sigma_{He^+}$ ratios of the individual fragmentation channels (Fig. 4). It is expected that this ratio is increasing towards higher degrees of ionization (see, e.g., Fig. 3). Indeed, the ratios form groups according to the degree of ionization of the molecule, and subgroups according to the degree of ionization of the oxygen atom. The ratio is an almost monotonic function of the energy of the proton fragment. It is seen that the multiple-ionization efficiency of the N^+ projectile relative to that of He^+ dramatically increases with the degree of ionization.

From the results of the fit we deduced the multiple-ionization cross sections of the water molecule as sums of the partial cross sections of the corresponding individual fragmentation channels. Single-ionization cross sections could not be determined with the present method. The main reason is that the nondissociative single-ionization events cannot be detected by our method at all (the recoil ion energy is far below our detection limit). Another reason is that in the 0.4–3-eV energy region, due to the strong overlap of the peaks, it is not possible to separate the heavy fragments from the light H^+ fragments originating from single ionization. Moreover, the kinetic energy of some of the fragments from ion-neutral breakups falls below our detection limit (0.4 eV).

Double ionization of the H_2O molecule may easily happen by removing both electrons from one of the O-H bonds. Accordingly, there is a rather large probability that one of the chemical bonds breaks, while the other remains unharmed. This can be the reason for the relatively large yield of the $OH^+ + H^+$ channel. For higher degrees of ionization both O-H bonds are likely to be affected. Therefore, the probability

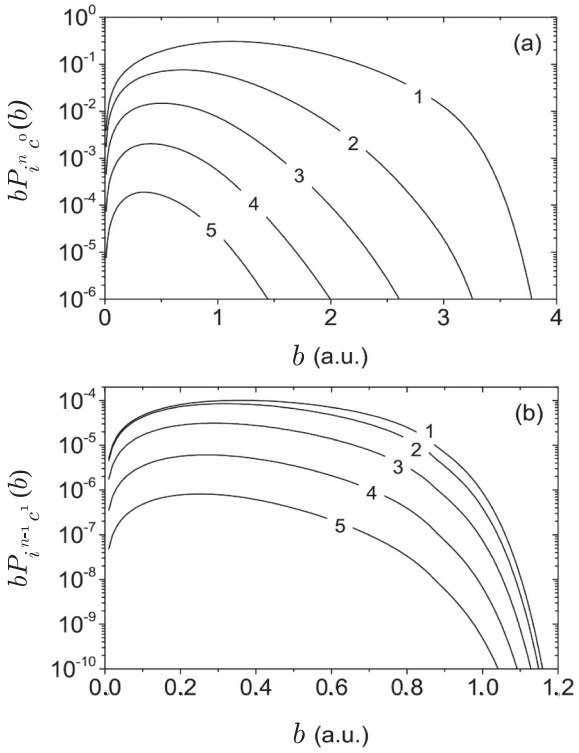

FIG. 5. (a) Ionization and (b) single capture + ionization probabilities as a function of the impact parameter for the $H^+ + H_2O$ collision system. The number of vacancies produced in the target molecule, n, is indicated at the curves.

of ion-pair breakups becomes negligible, and the molecule prefers to dissociate into three parts.

The experimentally obtained multiple-ionization cross sections (CSs) are compared to those calculated by the CTMC and CDW-EIS methods. Multiple-ionization data produced by the two theoretical methods are also compared with each other. The detailed description of the models is given in Refs. [28,30,33,34,34]. We found in our previous study [28] that CTMC provided good agreement with the measured double-differential electron emission cross sections for all the present collision systems. The results of the CDW-EIS calculations also reproduced the experimental double-differential electron emission cross sections for H^+ and He^+ projectiles, but they show significant deviations for N^+ impact. In the present work, we concentrate on the total probabilities and cross sections for ionization and electron capture. At this level, both theories predict that electron emission is dominated by single ionization.

In the following we analyze the multiple-target-vacancy production for water predicted by the two theories within the framework of the IPM. For a descriptive presentation we derive orientation-averaged $P_{i^n c^m}(b)$ values [see Eq. (1)] for n-fold ionization and simultaneous m-fold electron capture as a function of a scalar impact parameter b. This way, we can demonstrate and compare the approximate impact parameter dependence of the multiple-vacancy creation probabilities. In Fig. 5, we present CTMC results for n-fold ionization [Fig. 5(a)] and for singe-electron capture + $(n-1)$-fold ionization [Fig. 5(b)]. The averaged $bP_{i^n,c^0}(b)$ and $bP_{i^{n-1}c^1}(b)$

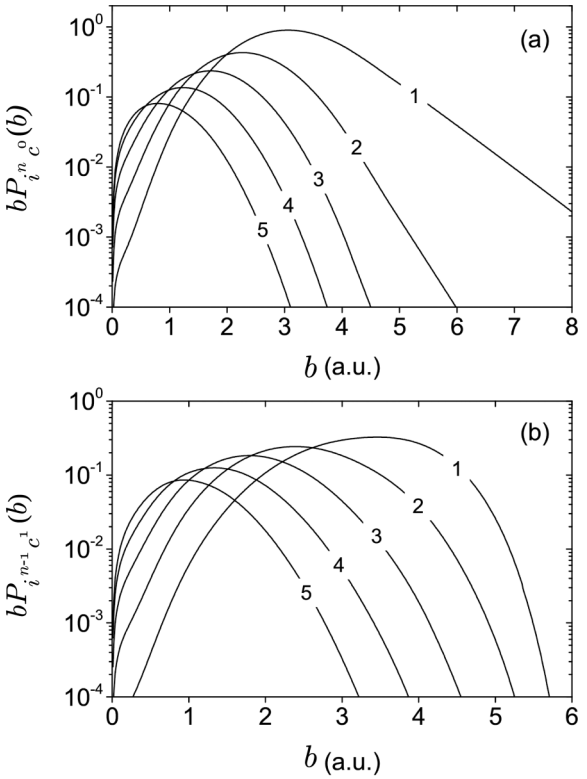

FIG. 6. (a) Ionization and (b) single capture + ionization probabilities as a function of the impact parameter for the $N^+ + H_2O$ collision system. The number of vacancies produced in the target molecule, n, is indicated at the curves.

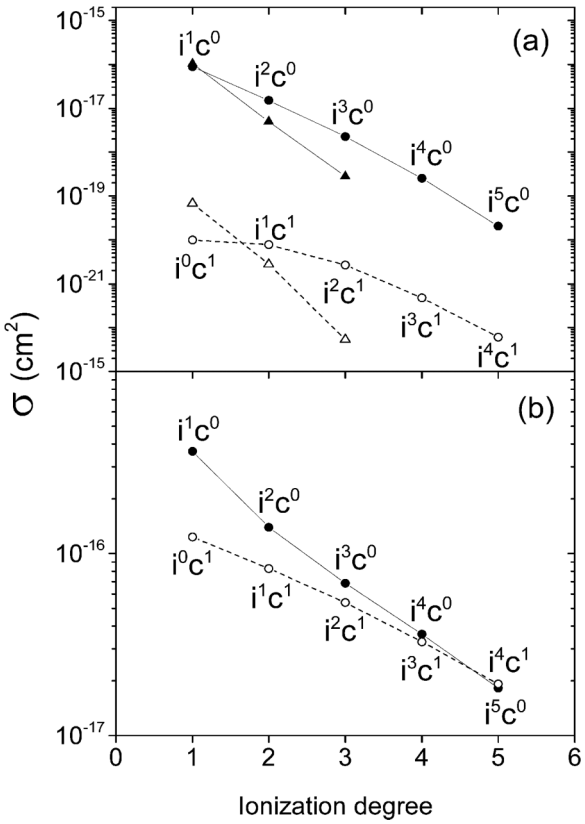

FIG. 7. Pure ionization (i^n c^0) and single capture + ionization (i^{n-1} c^1) cross sections for (a) H^+ and for (b) N^+ projectiles. Pure ionization is presented as solid circles for CTMC and solid triangles for CDW-EIS calculations. The capture + ionization process is denoted by open circles and open triangles for CTMC and CDW-EIS, respectively. The lines are a guide for the eye.

curves for H^+ impact on H_2O are plotted in Figs. 5(a) and 5(b), respectively. The impact parameter dependence of the same processes for N^+ impact is shown in Fig. 6. In the figures, the impact parameter is "measured" from the nucleus of the oxygen atom. Note that the areas under the $bP(b)$ curves are proportional to the cross sections of the particular processes.

According to the CTMC results for H^+ impact, single ionization is dominant in the full impact parameter region. The yields of higher degrees of ionization become more significant in narrower regions of smaller impact parameters [see Fig. 5(a)]. They remain much below the single-ionization yield everywhere. The maximum of the calculated $bP(b)$ curves decreases about three orders of magnitude from single to fivefold ionization. Single capture + ionization is limited to a small impact parameter range, and its contribution to vacancy production is negligible at all degrees of ionization. The shape of the $bP_{i^{n-1}c^1}(b)$ curves for different n are very similar to each other [see Fig. 5(b)].

The relevant impact parameter region for ionization is much larger for N^+ than for the H^+ projectile [see Fig. 6(a)]. Single ionization is also dominant here in the whole 1–8-a.u. impact parameter region with a maximum around 3 a.u. The multiple-ionization curves for N^+ impact extend to impact parameter ranges that are twice as large as those for proton impact. Similarly to H^+ impact, increasing degrees of ionization have smaller yields in gradually narrower windows at smaller impact parameters. However, the decrease of the yields is much weaker here: the maximum of the curve is only about one order of magnitude smaller for fivefold than for single ionization. Contrary to H^+ impact, multiple-ionization curves exceed that for single ionization at small impact parameters (below 2 a.u.). It shows that the effective perturbation strength increases towards smaller impact parameters. Moreover, it indicates that this is due to the screened potential of a $Z = 7$ central charge, which goes far above the ionic potential at small distances. This behavior is even more pronounced for the single capture + ionization process, as it is seen in Fig. 6(b).

The calculated multiple-vacancy production cross sections for H^+ and N^+ impact are shown in Fig. 7. According to the CTMC calculations the target ionization cross section for H^+ impact decreases more than three orders of magnitude from single to fivefold ionization. Cross sections calculated by CDW-EIS for single, double, and triple ionization are also presented in Fig. 7(a). They decrease faster with increasing degree of ionization than those obtained by the CTMC method. According to both theories the electron capture contribution to the vacancy production is negligible for the H^+ projectile. The yield of single-electron capture + ionization events remains at least two orders of magnitude lower than that of pure ionization, leading to the same number of vacancies.

For N^+ impact, the absolute cross sections are significantly larger, and their relative yields are strongly different from those of H^+ impact. The decrease of the cross section with increasing

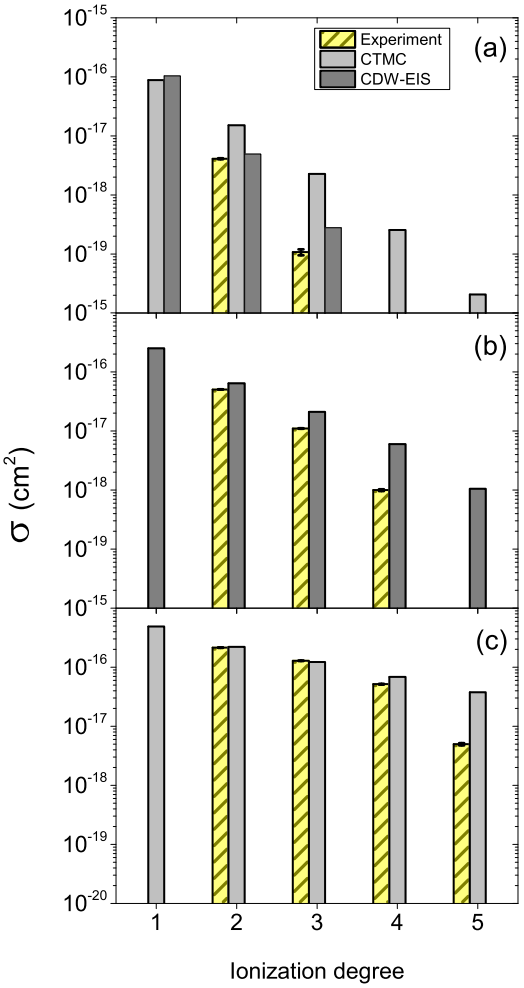

FIG. 8. Multiple-ionization cross section as a function of the ionization degree of the target for (a) H^+, (b) He^+, and (c) N^+ bombardment. The theoretical predictions for the different ionization degrees are also shown.

number of vacancies is much slower here: only one order of magnitude from single to fivefold ionization. Moreover, the role of electron capture is not negligible for N^+ impact. With increasing degree of target ionization the cross sections of the two processes approach each other. The cross section for single-capture + fourfold ionization even exceeds that of pure fivefold ionization [see Fig. 7(b)].

In Fig. 8, the experimentally determined multiple-ionization cross sections are compared with those obtained by CDW-EIS and CTMC calculations. For double-vacancy production, the CDW-EIS method provides a good agreement with experiment for both H^+ and He^+ impact at 1 MeV projectile energy. Moreover, there is a reasonably good agreement with the CDW-EIS method for the triple-vacancy yields, too. This quantum treatment seems to perform better than CTMC at high impact velocities and small perturbations, as it is seen for H^+ impact.

We could not measure single ionization in the present experiment directly. Nevertheless, we note that we have experimental information about it. In our earlier work [28] we measured the electron emission from the same collision systems and determined absolute double-differential cross sections for it. Those data have been compared with the results of both CDW-EIS and CTMC calculations at the level of double-differential spectra. Good agreement was found with CDW-EIS results for H^+ and He^+ impact, and with CTMC results for all three projectiles (H^+, He^+, and N^+). Therefore, we may also consider the theoretical predictions for single ionization as "semiexperimental" values.

For He^+ the CDW-EIS results also agree well with the measured multiple-target-ionization cross sections [see Fig. 8 (b)]. The agreement is as good as for proton impact in the case of double and triple ionization. However, the experimental fourfold-ionization cross section is far below the prediction of the theory. A slight fivefold-ionization cross section is also predicted but it was not found in the measurements. For the slowest N^+ projectile, the CTMC results practically coincide with the experiment up to triple ionization [see Fig. 8(c)]. For fourfold ionization, there is a slight deviation. Only the fivefold-ionization cross section is overestimated significantly. Since we compare absolute cross sections, this agreement is remarkable. We note that although the CDW-EIS calculations provided qualitative agreement with the measured electron emission yields for 46 keV/nucleon $N^+ + H_2O$ collisions [28], they have not been applicable for deducing multiple-ionization cross sections for that collision system.

A closer inspection of Fig. 8 shows a general tendency, namely, that the measured multiple-target-ionization cross sections decrease faster with the degree of ionization than the calculated data. It is true for both theoretical models. While for double-target ionization the calculations provide reasonable agreement with experiment, they both tend to gradually overestimate the experimental data towards higher ionization degrees. At four- and fivefold ionization this tendency becomes very strong. This increasing deviation of the calculated data from the experiment can be attributed to the limitations of the IPM. The role of electron correlation in electron emission increases with the degree of ionization. When a single-ionization probability is calculated with the first ionization potential as a parameter, the IPM is expected to overestimate the multiple-electron removal from the target.

Our data show that this overestimation is stronger if the perturbation is weak, and becomes less significant with strong perturbation. While for H^+ and He^+ projectiles the theories overestimate the cross section for $n = 3$, and dramatically overestimate it for $n = 4$, for N^+ impact the agreement is perfect for $n = 3$ and still reasonable for $n = 4$. It breaks down only at $n = 5$. This finding suggests that the importance of electron correlation may depend on the ratio of a mean correlation energy to a mean energy transfer characteristic for the collision.

V. SUMMARY AND CONCLUSIONS

We studied the fragmentation of H_2O molecules by the impact of 1 MeV-energy H^+ and He^+ and 0.65 MeV-energy N^+ projectiles. Single charged ions in this energy region are relevant for studying ion + H_2O collisions in the distal region of the Bragg peak. The energy and angular distribution of the emerging fragments were measured by a single-stage, parallel-plate-type, electrostatic spectrometer in a standard,

crossed-beam experiment. Absolute double-differential fragmentation cross sections of water were obtained for the three collision systems. The fragment energy spectra were fitted by Gaussian functions, and absolute cross sections for the particular fragmentation channels have been determined. From those channel yields we deduced the multiple-ionization cross sections for the water molecule and compared them with those calculated by CTMC and CDW-EIS methods.

The identification of the particular fragmentation channels is based on their experimental KER values published in the literature. We found that, up to fivefold ionization, the list of the fragmentation channels is close to complete. Moreover, we confirmed that a recent theoretical approach [27] provided correct identification and reasonable KER values for an important fraction of the fragmentation channels.

We found that the fragment ion emission was isotropic for all projectiles. The differential fragmentation cross section for N^+ is more than four times larger than that for He^+, and almost two orders of magnitude higher than that of H^+ in the entire fragment energy region. This strong variation of the yields is attributed to the increasing perturbation strength of the slower and slower projectile ions from H^+ to N^+. Besides the absolute differences between the cross sections, the relative ratios of the individual fragmentation channels are also different for the three projectiles, and additional channels appear for He^+ and even more for N^+ impact towards the high-energy end of the spectra. The presence of these fragmentation channels indicates that the maximum ionization degree increases from H^+ to N^+. It was found to be $q_{\max} = 3, q_{\max} = 4$, and $q_{\max} = 5$ for H^+, He^+, and N^+ impact, respectively.

The fragmentation cross-section spectrum for N^+ impact is very similar to those obtained by slow HCIs. This similarity indicates that the perturbation strength for the N^+ projectile can approach those for HCIs. This is partially due to the increase of the effective projectile charge in close collisions with the oxygen atom of the target. The dominance of low-impact-parameter events in the production of multiple ionized H_2O^{q+} molecular ions ($q = 2, \ldots, 5$) is confirmed by CTMC calculations.

The experimentally determined absolute multiple-ionization cross sections are in a general agreement with the results of the classical CTMC and the quantum-mechanical CDW-EIS calculations at lower degrees of ionization. At small perturbations the CDW-EIS method provides better agreement with experiments than the CTMC model. For N^+ impact, the nonperturbative character of the classical CTMC method gains importance. At this strong perturbation, the agreement between CTMC and experiment is remarkably good up to triple ionization, and it remains reasonable even for fourfold ionization.

Towards higher ionization states both theories systematically more and more overestimate the experimental cross sections. We attribute it to the limitations of the independent particle model, namely, the neglect of electron correlation within the IPM framework. In addition, we found that the overestimation is stronger if the perturbation is weak, and it becomes less significant with strong perturbation. For N^+ impact the agreement with experiment holds up to fourfold ionization. This finding suggests that the importance of electron correlation may depend on the ratio of a mean correlation energy to a mean energy transfer characteristic for the collision.

In conclusion, we studied the distal (i.e., low-energy) part of the Bragg peak in ion–water molecule collisions both experimentally and theoretically. We found that our CDW-EIS and CTMC models are able to provide a quantitative account for the multiple ionization of the target molecule in a wide range of the perturbation strength. We also gained information about the relative importance of electron correlation for weak and strong perturbations. We expect that a combined application of the tested theoretical methods will provide a satisfactory level of quantitative description in this focal region of different applications.

ACKNOWLEDGMENTS

This work has been supported by the Hungarian Scientific Research Foundation (OTKA Grant No. K109440), and by the National Information Infrastructure Program (NIIF). The authors thank the VdG-5 accelerator staff for the careful operation.

[1] M. N. Piancastelli, A. Hempelmann, F. Heiser, O. Gessner, A. Rüdel, and U. Becker, Phys. Rev. A **59**, 300 (1999).
[2] H. B. Pedersen, C. Domesle, L. Lammich, S. Dziarzhytski, N. Guerassimova, R. Treusch, L. S. Harbo, O. Heber, B. Jordon-Thaden, T. Arion, M. Förstel, M. Stier, U. Hergenhahn, and A. Wolf, Phys. Rev. A **87**, 013402 (2013).
[3] G. Dujardin, D. Winkoun, and S. Leach, Phys. Rev. A **31**, 3027 (1985).
[4] A. L. F. de Barros, J. Lecointre, H. Luna, M. B. Shah, and E. C. Montenegro, Phys. Rev. A **80**, 012716 (2009).
[5] F. Frémont, C. Leclercq, A. Hajaji, A. Naja, P. Lemennais, S. Boulbain, V. Broquin, and J.-Y. Chesnel, Phys. Rev. A **72**, 042702 (2005).
[6] H. Luna, A. L. F. de Barros, J. A. Wyer, S. W. J. Scully, J. Lecointre, P. M. Y. Garcia, G. M. Sigaud, A. C. F. Santos, V. Senthil, M. B. Shah, C. J. Latimer, and E. C. Montenegro, Phys. Rev. A **75**, 042711 (2007).
[7] H. Luna, E. G. Cavalcanti, J. Nickles, G. M. Sigaud, and E. C. Montenegro, J. Phys. B **36**, 4717 (2003).
[8] I. Ben-Itzhak, K. D. Carnes, D. T. Johnson, P. J. Norris, and O. L. Weaver, Phys. Rev. A **49**, 881 (1994).
[9] P. M. Y. Garcia, G. M. Sigaud, H. Luna, A. C. F. Santos, E. C. Montenegro, and M. B. Shah, Phys. Rev. A **77**, 052708 (2008).
[10] F. Alvarado, R. Hoekstra, and T. Schlathölter, J. Phys. B **38**, 4085 (2005).
[11] U. Werner, K. Beckord, J. Becker, H. O. Folkerts, and H. O. Lutz, Nucl. Instrum. Methods Phys. Res. Sect. B **98**, 385 (1995).
[12] J. Rajput and C. P. Safvan, Phys. Rev. A **84**, 052704 (2011).
[13] P. Sobocinski, Z. D. Pesic, R. Hellhammer, D. Klein, B. Sulik, J.-Y. Chesnel, and N. Stolterfoht, J. Phys. B **39**, 927 (2006).

[14] E. C. Montenegro, M. B. Shah, H. Luna, S. W. J. Scully, A. L. F. Barros, J. A. Wyer, and J. Lecointre, Phys. Rev. Lett. **99**, 213201 (2007).
[15] H. Luna and E. C. Montenegro, Phys. Rev. Lett. **94**, 043201 (2005).
[16] D. Schardt. T. Elsässer, and D. Schulz-Ertner, Rev. Mod. Phys. **82**, 383 (2010).
[17] H. Paul and A. Schinner, At. Data Nucl. Data Tables **85**, 377 (2003).
[18] S. W. J. Scully, J. A. Wyer, V. Senthil, M. B. Shah, and E. C. Montenegro, Phys. Rev. A **73**, 040701 (2006).
[19] I. Ben-Itzhak, K. D. Carnes, S. G. Ginther, D. T. Johnson, P. J. Norris, and O. L. Weaver, Phys. Rev. A **47**, 3748 (1993).
[20] U. Werner, J. Becker, T. Farr, and H. O. Lutz, Nucl. Instrum. Methods Phys. Res. Sect. B **124**, 298 (1997).
[21] M. Tarisien, L. Adoui, F. Frémont, D. Lelièvre, L. Guillaume, J.-Y. Chesnel, H. Zhang, A. Dubois, D. Mathur, S. Kumar, M. Krushnamurthy, and A. Cassimi, J. Phys. B **33**, L11 (2000).
[22] B. Seredyuk, R. W. McCullough, H. Tawara, H. B. Gilbody, D. Bodewits, R. Hoekstra, A. G. G. M. Tielens, P. Sobocinski, D. Pesic, R. Hellhammer, B. Sulik, N. Stolterfoht, O. Abu-Haija, and E. Y. Kamber, Phys. Rev. A **71**, 022705 (2005).
[23] P. Sobocinski, Z. D. Pesic, R. Hellhammer, N. Stolterfoht, B. Sulik, S. Legendre, and J.-Y. Chesnel, J. Phys. B **38**, 2495 (2005).
[24] Z. D. Pesić, J.-Y. Chesnel, R. Hellhammer, B. Sulik, and N. Stolterfoht, J. Phys. B **37**, 1405 (2004).
[25] Z. D. Pesić, R. Hellhammer, B. Sulik, and N. Stolterfoht, J. Phys. B **42**, 235202 (2009).
[26] G. H. Olivera, C. Caraby, P. Jardin, A. Cassimi, L. Adoui, and B. Gervais, Phys. Med. Biol. **43**, 2347 (1998).
[27] W. Wolff, H. Luna, R. Schuch, N. D. Cariatore, S. Otranto, F. Turco, D. Fregenal, G. Bernardi, and S. Suarez, Phys. Rev. A **94**, 022712 (2016).
[28] S. T. S. Kovács, P. Herczku, Z. Juhász, L. Sarkadi, L. Gulyás, and B. Sulik, Phys. Rev. A **94**, 012704 (2016).
[29] Á. Kövér, Gy. Szabó, D. Berényi, D. Varga, I. Kádár, S. Ricz, and J. Végh, Phys. Lett. A **89**, 71 (1982).
[30] L. Sarkadi, P. Herczku, S. T. S. Kovács, and Á. Kövér, Phys. Rev. A **87**, 062705 (2013).
[31] E. Lattouf, Z. Juhász, J.-Y. Chesnel, S. T. S. Kovács, E. Bene, P. Herczku, B. A. Huber, A. Méry, J.-C. Poully, J. Rangama, and B. Sulik, Phys. Rev. A **89**, 062721 (2014).
[32] E. W. Kuipers and A. L. Boers, Nucl. Instrum. Methods Phys. Res. Sect. B **29**, 567 (1987).
[33] L. Sarkadi, Phys. Rev. A **92**, 062704 (2015).
[34] L. Gulyás, I. Tóth, and L. Nagy, J. Phys. B **46**, 075201 (2013).
[35] L. Gulyás, S. Egri, H. Ghavaminia, and A. Igarashi, Phys. Rev. A **93**, 032704 (2016).
[36] D. S. F. Crothers and L. J. Dube, Adv. At. Mol. Opt. Phys. **30**, 287 (1992).
[37] N. Stolterfoht, R. D. DuBois, and R. D. Rivarola, *Electron Emission in Heavy Ion-Atom Collisions* (Springer, Berlin, 1997).
[38] G. H. Olivera, P. D. Fainstein, and R. D. Rivarola, Phys. Med. Biol. **41**, 1633 (1996).
[39] C. A. Tachino, J. M. Monti, O. A. Fojón, C. Champion, and R. D. Rivarola, J. Phys. B **47**, 035203 (2014).
[40] J. M. Monti, R. D. Rivarola, and P. D. Fainstein, J. Phys. B **44**, 195206 (2011).
[41] C. Illescas, L. F. Errea, L. Méndez, B. Pons, I. Rabadán, and A. Riera, Phys. Rev. A **83**, 052704 (2011).
[42] A. E. S. Green, D. L. Sellin, and A. S. Zachor, Phys. Rev. **184**, 1 (1969).
[43] R. H. Garvey, C. H. Jackman, and A. E. S. Green, Phys. Rev. A **12**, 1144 (1975).
[44] C. O. Reinhold and C. A. Falcón, Phys. Rev. A **33**, 3859 (1986).
[45] P. J. Richardson, J. H. D. Eland, P. G. Fournier, and D. L. Cooper, J. Chem. Phys. **84**, 3189 (1986).